photonics

MDPI

Review

Optical Trapping, Sensing, and Imaging by Photonic Nanojets

Heng Li, Wanying Song, Yanan Zhao, Qin Cao and Ahao Wen *

Institute of Nanophotonics, Jinan University, Guangzhou 511443, China; liheng@stu2019.jnu.edu.cn (H.L.); songwanying2019@stu2019.jnu.edu.cn (W.S.); zhaoyanan@stu2020.jnu.edu.cn (Y.Z.); caoqin@jnu.edu.cn (Q.C.)
* Correspondence: wenahao3@jnu.edu.cn

Abstract: The optical trapping, sensing, and imaging of nanostructures and biological samples are research hotspots in the fields of biomedicine and nanophotonics. However, because of the diffraction limit of light, traditional optical tweezers and microscopy are difficult to use to trap and observe objects smaller than 200 nm. Near-field scanning probes, metamaterial superlenses, and photonic crystals have been designed to overcome the diffraction limit, and thus are used for nanoscale optical trapping, sensing, and imaging. Additionally, photonic nanojets that are simply generated by dielectric microspheres can break the diffraction limit and enhance optical forces, detection signals, and imaging resolution. In this review, we summarize the current types of microsphere lenses, as well as their principles and applications in nano-optical trapping, signal enhancement, and super-resolution imaging, with particular attention paid to research progress in photonic nanojets for the trapping, sensing, and imaging of biological cells and tissues.

Keywords: microspheres; photonic nanojets; optical trapping; signal enhancement; super-resolution imaging

Citation: Li, H.; Song, W.; Zhao, Y.; Cao, Q.; Wen, A. Optical Trapping, Sensing, and Imaging by Photonic Nanojets. *Photonics* **2021**, *8*, 434. https://doi.org/10.3390/photonics8100434

Received: 30 August 2021
Accepted: 1 October 2021
Published: 11 October 2021

1. Introduction

Optics are widely used in modern life and production, and are one of the frontier sciences in the field of modern science. Trapping [1–5], imaging [6–10], and sensing [11–15] nanoscale objects with light are becoming more important in nano-photonics and biomedicine. In 1590, Dutch eyeglass craftsman Hans Janssen and his son Zaccharias invented the first optical microscope, thereby breaking the limit of what the human eye could observe. With improvements by Leeuwenhoek and other scientists, optical microscopes have played a pivotal role in biological sciences, materials science, and other fields, leading to higher expectations for imaging resolution. In 1873, German physicist Abbe [16] discovered the formula for the resolution limit of a microscope: $d = \lambda/2n\sin\theta$, in which λ is the wavelength of illumination light, n is the refractive index of the imaged medium, and θ is the half angle at which the object receives the light from the object. When the illumination source is visible light, the resolution of the optical microscope is approximately 200 nm. In other words, if the distance between two points reaches 200 nm, it is not distinguishable by an optical microscope, which limits the development and progress of science. Similarly, the focused beam of optical tweezers also has a diffraction limit. Optical tweezers rely on a high numerical aperture. When particles with a diameter of less than 200 nm are in a focused beam, it is difficult to sense the gradient of light intensity. Therefore, it is difficult for optical tweezers to stably trap objects that are on the order of nanometers (<200 nm).

Researchers have recently made attempts to overcome the diffraction limit of traditional microscopes and optical tweezers [17–21]. Scanning electron microscopy (SEM) and transmission electron microscopy (TEM) have high resolution [22,23], and yet, the samples must be placed in a vacuum environment, which is not suitable for studying living biological samples. Fluorescence microscopy allows for the imaging of fluorescently labeled biological cell structures [24,25], enabling super-resolution imaging on the order of a few to several tens of nanometers. However, this technology requires the binding of fluorescent probes to the protein of the target sample, so only one type of protein can be

imaged at a time. Additionally, the fluorescence intensity of the sample is easily extinguished over time. In 1972, Ash et al. obtained super-resolution microscopic images under an evanescent wave condition for the first time with a scanning near field microscope [26]. Soon after, researchers used a scanning near-field microscope with an optical probe tip close to the sample surface, scanning point-by-point in the near-field region, thus breaking the diffraction limit to obtain optical information on the sample surface [27,28]. At the same time, this approach takes a long time to obtain a complete image and it cannot be used to observe the sample in real time. To propagate the evanescent wave carrying sub-wavelength information to the far field, Pendry theoretically proposed a negative refractive index medium to enhance the evanescent wave to achieve sub-wavelength resolution, which provides the possibility to collect information in the far field [29]. Many researchers have used silver and other precious metal materials to prepare plasmon superlenses on this basis [30–33]. In recent years, plasmons have also been applied to the fields of optical trapping and optical manipulation [34–36]. When the wavelength of incident light irradiates the interface between the metal and medium, the free electrons on the metal surface oscillate. Resonance will occur when the wavelength of the incident light matches the resonant wavelength of the surface plasmon [37,38]. Under such resonance conditions, the energy of the electromagnetic field will be transformed into the collective vibrational energy of free electrons on the metal surface, and the light will be confined to the sub-wavelength range of the metal surface and be greatly enhanced. Similarly, photonic crystals were introduced to better break the diffraction limit and stably capture nanoparticles [39]. The coupling of the photonic crystal cavity and the laser makes the light intensity in the cavity increase, and the light force received by the nanoparticles becomes larger. However, for the optical trapping, imaging, and sensing of plasmon optical tweezers and photonic crystal optical tweezers, the absorption of light by the metal substrate can easily cause local thermal effects, thereby destroying the stability of the trap. More importantly, when the nanoparticles are biomaterials, the high temperature generated by the thermal effect will destroy the activity of biomolecules.

Compared with these complex technologies, microlens technology has been widely developed in the fields of super-resolution imaging [40], biosensing [41], and optical trapping [42] on the basis of its simplicity of preparation, ease of manipulation, and it being label-free. In 2004, the local photonic nanojet generated by the shadow surface of a micrometer-scale circular medium cylinder illuminated by a plane wave was first proved by Chen et al. By using high-resolution finite difference time domain (FDTD) numerical simulations, they found that the waist of the photonic nanojet is smaller than the diffraction limit, and it can propagate at multiple wavelengths without significant diffraction [43]. In 2011, Wang et al. [44] first reported microsphere lens nanoscopy that combines micron-scale transparent dielectric SiO_2 microspheres with conventional optical microscopy. The nanoscopy surpassed the diffraction limit under white light conditions to obtain optical imaging with 50 nm resolution. This simple and effective method can convert a near-field evanescent wave with high-frequency spatial information into propagation modes [45–47], offering the possibility to trap and detect nanoparticles [48–51], enhance the signal [52–55], mediate backaction force [56], and improve the performance of optical systems [57,58]. In this article, we will summarize the recent research progress of microsphere lenses, introduce three types of microsphere lenses, focus on the applications of microsphere lenses in optical trapping, sensing, and imaging, and discuss potential application scenarios.

2. Types and Principles of Microsphere Superlenses

2.1. Types of Microspheres

Microsphere superlenses can be classified by the medium in which the microspheres exist: microspheres in air medium, microspheres in liquid medium, and microspheres in solid medium.

In 2011, SiO_2 microspheres with a refractive index of 1.46 and diameter of 2–9 μm were directly placed on the surface of a sample by self-assembly technology to achieve super-resolution imaging of gold-plated oxide anodic alumina film with a spacing of 50 nm under a light source with a wavelength of 600 nm [44], as shown in Figure 1a. The microsphere lens allows for the collection of information about the object in the near field and the formation of a magnified virtual image in the far field. A resolution of $\lambda/8$–$\lambda/14$ and a magnification of $\times 8$ can be achieved in the air medium. In addition, according to theoretical calculations, the super-resolution intensity of microspheres with a refractive index of 1.8 was greatest in air. When the refractive index increases to 2.0, the super-resolution capability of microspheres becomes smaller. This demonstrates that not all microspheres have super-resolution capabilities; only microspheres that meet specific conditions can generate photonic nanojets to achieve super-resolution imaging. Microspheres in liquid media can be classified into two groups: semi-immersed in liquid and fully immersed in liquid. The experimental setup diagram is shown in Figure 1b [59]. Hao et al. showed that when SiO_2 microspheres with a refractive index of 1.47 and diameter of 3 μm were completely submerged in an ethanol solution, the microspheres did not have super-resolution capabilities [60]. When part of the ethanol solution was volatilized and the microspheres were semi-submerged in the solution, the contrast and resolution of the virtual image of the tested sample were enhanced, allowing imaging of commercial blue light discs with a width of 100 nm. When the ethanol solution was nearly evaporated and the microspheres were exposed to air, the resolution became weaker, further demonstrating that semi-immersion of the microspheres in liquid could improve the resolution of imaging. However, the volatility of the ethanol solution was not conducive to a prolonged observation of the experiment. Darafsheh et al. then demonstrated that super-resolution imaging can be achieved when high refractive index microspheres were completely submerged in a liquid solution [61,62]. Barium titanate ($BaTiO_3$) microspheres with a refractive index of 1.9 were completely submerged in an isopropyl alcohol solution with a refractive index of 1.37, and the super-resolution imaging of two-dimensional gold nanodimers comprising gold nanopillars with a diameter of 120 nm and height of 30 nm was achieved under an illumination light source with a wavelength of 550 nm. In 2014, the team demonstrated that the imaging effect $BaTiO_3$ microspheres with a refractive index of 2.1 submerged in an isopropane alcohol solution was better than that of soda lime glass with a refractive index of 1.51 in air [63]. Moreover, Darafsheh et al. proved that high refractive index microspheres embedded in a transparent film can achieve super-resolution imaging [64]. The experimental setup of microspheres in a solid medium is shown in Figure 1c. $BaTiO_3$ microspheres with a refractive index of 1.9 were self-assembled and distributed on liquid polydimethylsiloxane (PDMS). After drying and other steps to form PDMS films, the films embedded with microspheres were placed on the sample, and an illumination source of 550 nm was passed through the film to form a magnified virtual image below the specimen in the reflection illumination mode with a resolution of up to $\lambda/4$. Overall, microspheres with low refractive index can be directly imaged in air medium, and microspheres with high refractive index can be imaged at super-resolution in liquid and solid media. The microspheres in the liquid are flexible and can be trapped and manipulated with the help of auxiliary tools, such as optical fibers, to realize the imaging and sensing of specific particles and positions. The microspheres in the film can be prepared in advance and used as a cover glass for the sample, which can avoid the evaporation of liquid in the experiment and improve the stability of imaging.

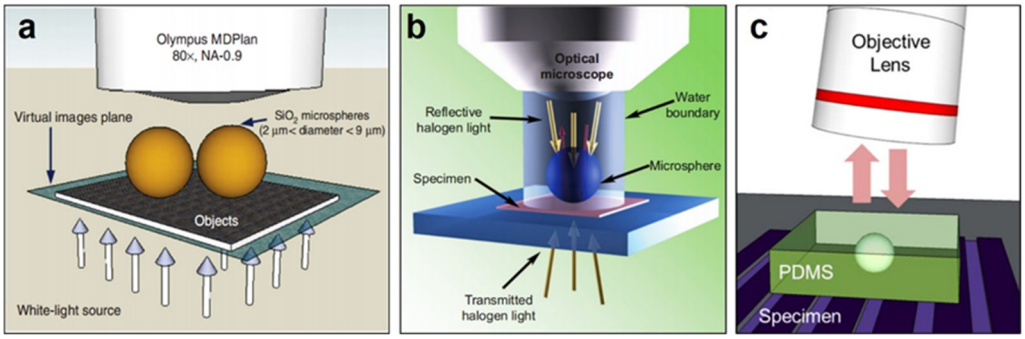

Figure 1. Schematic diagram of different microsphere superlens experimental setups. Schematic diagrams of the device with microspheres in an (**a**) air medium, (**b**) liquid medium, and (**c**) solid medium.

2.2. Principles of Photonic Nanojets for Optical Trapping, Sensing and Imaging

The optical properties of the photonic nanojets [65], whispering gallery mode [66], and directional antenna [67] of the microsphere lens enhance the interaction between photons and matter, thereby improving the ability of optical trapping, sensing, and imaging. The imaging of a conventional optical microscope comprises light spots formed by light and dark streaks. When two objects that are close pass through the lens, the diffracted light spots will overlap and be indistinguishable. Therefore, the resolution of conventional optical microscope depends on the size of the spot produced by focusing the incident light on the far field, which is limited by diffraction. For particle scales less than one-tenth of a wavelength, the scattered light intensity in each direction of the particle is not the same and is prone to Rayleigh scattering; the scattering cross section increases with the refractive index, and the electric field intensity increases with the refractive index in the near field range. When the particle scale is larger than the wavelength, Mie scattering will dominate and the microsphere will focus the incident beam into a photonic nanojet with a small width and high intensity [68,69]. The mechanism of the optical trapping, sensing, and imaging of microlens is usually explained by the photonic nanojet. The evanescent wave close to the surface of the microsphere plays an important role in the process of imaging the microsphere in conjunction with an optical microscope [70]. The sample is magnified by the microsphere lens, and then magnified twice by the microscope. The imaging mechanism of the microsphere lenses is shown in Figure 2a. The incident light can be considered a beam of parallel light when the incident waves irradiate the surface of the microsphere in the far-field range, and the distance between the sample and the wavelength of the light source are the same order of magnitude. When the parallel light passes through the surface of the microlens, it forms different angles of incidence, and then enters the interior through refraction. At this time, the evanescent wave carrying the high spatial frequency information of the object is converted into a propagating wave in the microsphere, which is received by a traditional optical microscope, and an enlarged virtual image can be produced in the far field [71]. In 2005, Li et al. demonstrated that the nano-photonic nanojet and backscattering capabilities of the microspheres were enhanced through FDTD simulation [72]. This shows that the microsphere lenses focus the light on the sub-diffraction limited size, realizes super-resolution imaging, and traps and senses particles to enhance the spectral signal [73,74]. Using an innovative 3D mapping technique, researchers have discovered significant field intensification around the poles of dielectric microspheres by tracking field-lines passing the critical points of the Poynting vector distribution [75].

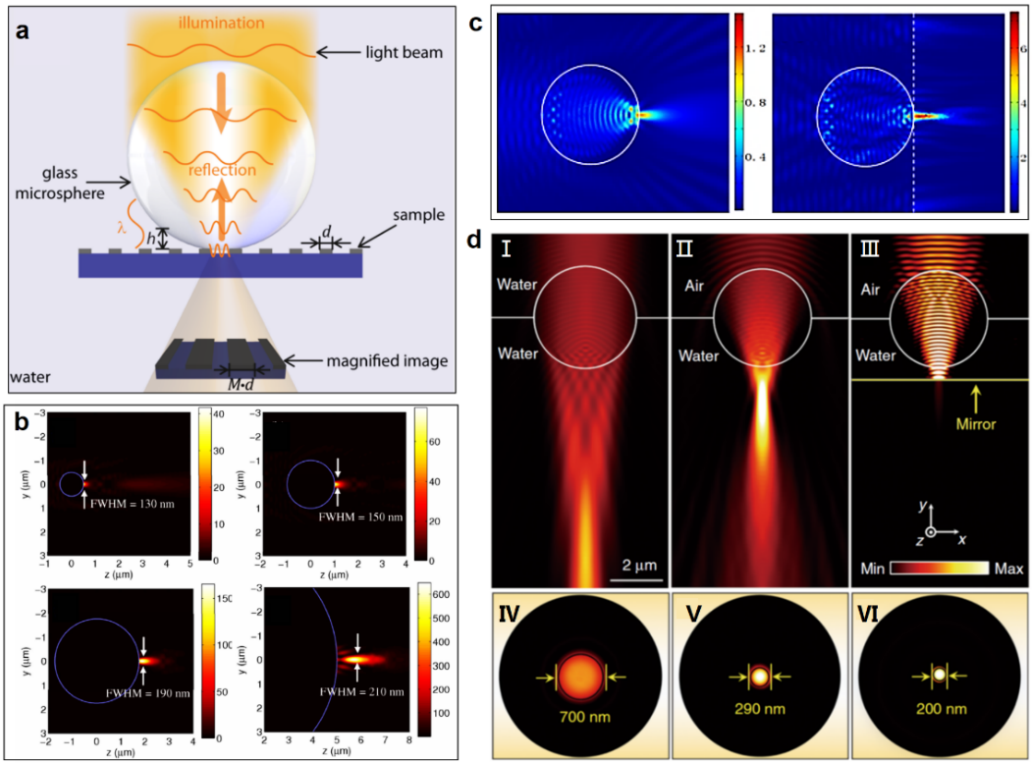

Figure 2. Principle of photonic nanojet generation. (**a**) Imaging schematic diagram of a grating sample using a microsphere superlens; (**b**) The near-field intensity and FWHM of the photonic nanojet generated by microspheres with diameters of 1.0 μm, 2.0 μm, 3.5 μm, and 8.0 μm; (**c**) Theoretical simulation of the light field distribution of microspheres on air and a Si substrate; (**d**) Optical intensity distributions of light focusing and light spots by a microlens fully immersed in water, semi-immersed in water, and suspended on the surface of a mirror.

The focusing ability of the photonic nanojet is related to the diameter and refractive index of the microspheres. Figure 2b shows the microsphere irradiated with a plane wave with a wavelength of 400 nm, in which the shadow side of the dielectric particles focuses a high-intensity photonic nanojet. Microspheres with different diameters were simulated by a finite element method. With the increase in diameter, the maximum light intensity and a full width at half maximum (FWHM) of the microspheres gradually increased; yet, the microspheres better convert evanescent waves into propagation waves the farther away the focus position is from the surface of the microspheres, and the high intensity energy carries more subwavelength information [72]. The refractive index of the microspheres also affects the imaging resolution. When the parallel light passes through the microspheres with high refractive index ($n > 2$), the focus is generated in the microspheres, so it is impossible to perform super-resolution imaging of the object. When the light passes through the microspheres with low refractive index ($1 < n < 2$), the focus is out of the microspheres, and the super-resolution imaging of the object can be performed [48]. Lee et al. also performed simulations using the Mie theory and found that the larger the refractive index of the microsphere [76], the stronger the intensity of the photonic nanojet. Additionally, the closer the strongest light intensity is to the surface of the microsphere, the higher the resolving power of the microsphere. The presence or absence of a substrate beneath the microsphere affects the formation of the shape and size of the photonic nanojets. As shown in Figure 2c, the incident light focuses near the shadow surface of the microsphere, forming a photonic nanojet with a focusing width of 150 nm. When the microsphere contacts the Si substrate, the electric field is redistributed around the sphere, and the formed photonic nanojet passes through the substrate with a focusing width of approximately 120 nm [77]. The properties of the photonic nanojet generated by the dielectric microspheres will change

or even disappear for different substrate materials, leading to changes in the signal. In 2014, Sundaram's team further proved the importance of the substrate material on the imaging results by comparing the imaging resolution of microspheres selected without substrate, with aluminum oxide substrate materials and fused silica substrate materials [78]. As shown in Figure 2d, the intensity of the light field produced by the microlens is different in different environments [79]. When the 560 nm illuminating light is irradiated on the fully immersed microlens, the output light is focused on the far field with a focal length is 7.0 μm, and a relatively large output spot is produced. When the middle of the microlens is placed at the air–water interface, the output light is highly focused in the near field with a focal length of 0.7 μm, forming a tiny spot. When the distance between the microlens and the mirror substrate is 300 nm, the intensity of the light spot is generated by the light increases. This is due to the enhanced coherent interference between the photonic nanojet of the microlens and the reflected light from the specular surface.

In addition to spherical microlens, structures such as dielectric cubes, asymmetric cuboids, nanohole structured mesoscale dielectric spheres, and cylindrical objects can generate photonic nanojet, improve the spatial resolution of the imaging system, and even change the direction and focusing characteristics of the photonic nanojet to manipulate, sense, and image nanoscale objects [80–86]. The cuboid solid immersion lens can generate photonic nanojets though transmission and reflection modes to enhance the lateral resolution of the optical system [87]. When the dielectric cube is placed at the focus imaging point of the continuous wave terahertz imaging system or placed on the substrate, the spatial resolution of the imaging system can also be effectively improved [88,89]. Nguyen et al. placed a Teflon cube with a refractive index of 1.46 at the imaging point of the terahertz imaging system. After passing through the enhancer, the image contrast increased by a factor of 4.4. Besides, Ang et al. [90] attached a triangular prism to the irradiated surface of the cube. Due to the varying in the thickness of the prism, the phase of the transmitted waves in the upper and lower parts of the system changed, the electric field intensity became non-symmetric, showing concave deformation, which formed a curved photonic nanojet near the shadow surface. At the same time, the intensity of the photonic nanojet generated by the asymmetric cuboids was higher than that generated by cuboids and caused gold nanoparticles to move in a curved trajectory in the transmitted field (Figure 3a), to avoid obstacles. The shape and structure of the lens will also affect the length of the photonic nanojets. In recent years, researchers have changed the microstructure of the lens to obtain longer photonic nanojets. As shown in Figure 3b, Zhu et al. [91] obtained the ultra-long photonic nanojet by using the characteristics of the asymmetric two-microstructure formed by the support stage and the spherical cap. By appropriately adjusting the radius of curvature of the curved surface, an arbitrary elongated photonic nanojet can be obtained. Furthermore, the cascaded asymmetric silica microstructure will produce stable optical transmission and a FWHM waist close to $\lambda/4$. Gu et al. [92] used a plane wave to irradiate a liquid-filled hollow microcylinder to obtain the longest photonic nanojets. Immersion of the liquid-filled hollow cylinder into the solution environment can greatly spread the light beam. Because of the refractive index difference between the filling liquid and the immersion liquid, the focal length, attenuation length, and FWHM of the photonic nanojet can be flexibly adjusted by changing the inner filling liquid. Moreover, the permittivity contrast between the nanohole material and the dielectric particle results in the electric field enhancement of the nanohole-structured electric microspheres, which can produce high optical power and electric field intensity in the low refractive index hole material (air) [93–96]. In other words, a nanohole created on the back surface of a mesoscale particle in the medium can localize the field characteristics of the photonic nanojet to the size of the nanohole, thereby improving the resolution. As shown in Figure 3c, the focal spot size and focal volume of the nano-structured microspheres with a through hole of diameter $\lambda/5$ is larger than that without nanoholes. The larger nanoholes of $\lambda/5$ weaken the focusing ability of the dielectric microspheres. When the hole size is reduced by $\lambda/10$ or $\lambda/15$, the focal spot size and focal volume are significantly reduced. Similarly, dielectric microspheres

with blind hole of diameter $\lambda/5$ on the surface, its focus ability are also weakened by the hole. When the aperture is reduced to below $\lambda/10$, the focused light spot is mainly limited to the blind hole.

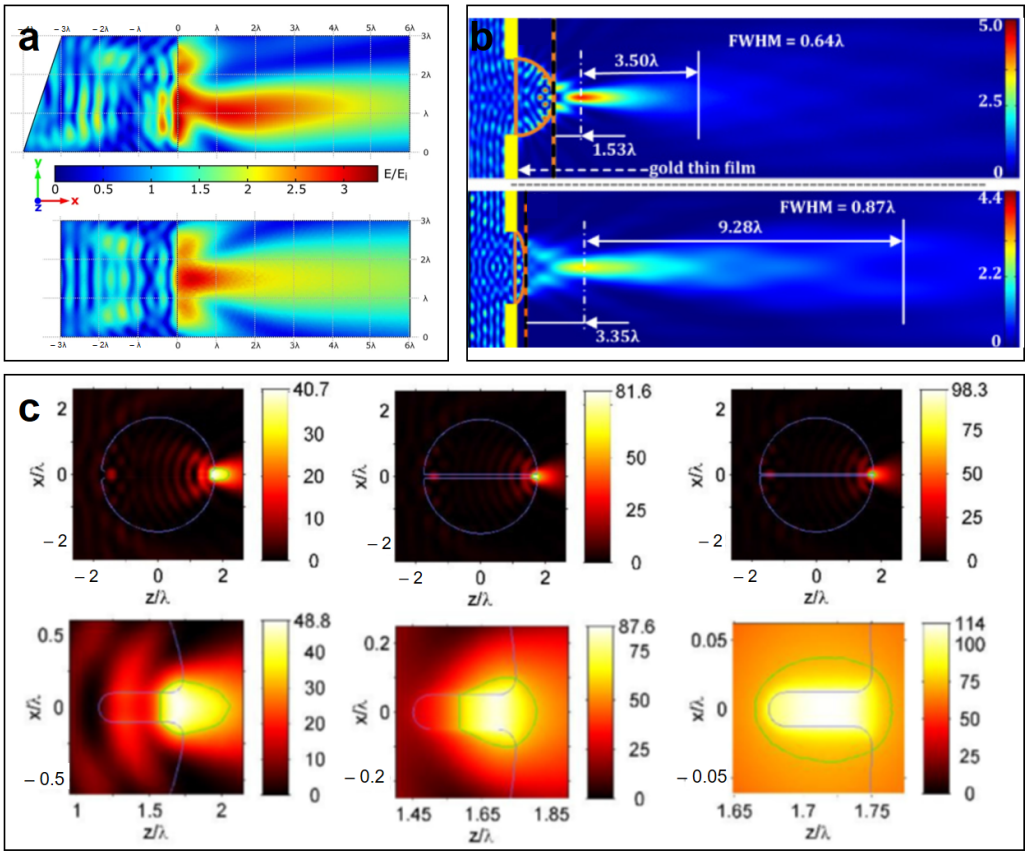

Figure 3. Generation of photonic nanojet of microlens with different structures. (**a**) Intensity of light field generated by asymmetric cuboids and cubes; (**b**) Spatial intensity distribution of structures with radius of curvature of 2λ and 4λ; (**c**) Light intensity of the simulated dielectric microspheres with a nanohole of size $\lambda/5$, $\lambda/10$, $\lambda/15$ and dielectric microspheres with a blind nanohole of the diameter $\lambda/5$, $\lambda/10$, $\lambda/40$.

Furthermore, the electromagnetic mode of objects also plays a crucial role in optical trapping, sensing, and imaging [97,98]. Using the whispering gallery mode can improve the imaging resolution and the possibility of particle detection. In the process of collecting point source information in whispering gallery mode, each external mode has an organized spatial spectrum, which can form an imaging mode with less than half of the illumination wavelength. When the object to be measured is close to the microsphere cavity, changes occur around the microsphere cavity, disturbing the whispering gallery mode. By receiving the resonant wavelength generated by the micro-cavity to obtain the change of the resonant frequency, the conversion of the evanescent wave to the propagating wave can be enhanced, and the corresponding external mode can be improved, so as to realize the detection of the refractive index of the surrounding environment or the concentration of molecules, as well as higher resolution imaging [99].

3. Optical Trapping and Sensing Using Photonic Nanojets

3.1. Fluorescence Signal Enhancement of Trapped Nano-Objects

Microsphere lenses can enhance the interaction of photons with matter under incident light irradiation, significantly enhancing the fluorescence signal [100,101] and sensing of the signal of manipulated objects in real time, providing a convenient method for nanomaterial characterization and biomolecular diagnosis. In 2015, Yang et al. probed the fluorescence signal of nanoparticles in microfluidic channels. When the nanoparticles pass through 3 μm melamine microspheres on a microcirculation channel, the photonic nanojets generated by the microsphere array are able to be transported in the flow medium and the fluorescence intensity of the nanoparticles is enhanced, such that the immune complexes formed on the Au nanoparticles can be detected [102].

However, most microsphere lenses cannot be adjusted and manipulated in the sample pool to detect objects. Lu et al. proved that the photonic nanojet generated by optical trapped microspheres can provide greater light power, making it easier to trap single 10 nm upconversion fluorescence nanoparticle (UCNP) [103]. The particles can be trapped and sensed by optical forces from fiber tweezers or by photophoresis [104–108]. As shown in Figure 4a, three-dimensional trapping and sensing the object can be implemented by combining optical fibers with microspheres [109]. Li et al. modified polystyrene (PS) microspheres or TiO_2 microspheres to adhere to the end face of negatively charged fiber tweezers. When trapping microlenses using fiber tweezers, the microlens generates a high-intensity photonic nanojet that manipulates the nanoparticles, which then acts as a high-value aperture objective for collecting the signal, and the fluorescent signal of the nanoparticles is enhanced when being sensed by the microlens adhered to the fiber tip. When sensing single nanoparticles in the presence of PS and TiO_2 microlenses, the fluorescence intensity of the trapped nanoparticles is 20 times and 30 times greater than the fluorescence intensity sensed by bare optical fibers, respectively. The excitation light passing through the microlens can produce a photonic nanojet phenomenon, in which the electric field intensity is enhanced in the local spot generated by the photonic nanojet, and this enhanced electric field contributes to the fluorescence excitation rate [110].

Dielectric microspheres act as microlenses to enhance fluorescence signals, and biological probes for the sensing and imaging of fluorescence signals from particles and biological tissues are also gradually being developed [111–113]. In 2017, Li et al. [114] used spherical yeast as a natural bio-microlens to enhance upconversion fluorescence, as shown in Figure 4b. The optical fiber is placed in the UCNPs. A laser with a wavelength of 980 nm and an optical power of 3 mW was emitted into the optical fiber. The fluorescence excited by the bare optical fiber was weak. The fluorescence intensity of the UCNPs was significantly enhanced when using fiber tweezers to trap the microlens. The use of a biological microlens can trap *Escherichia coli* (*E. coli*) and *Staphylococcus aureus* (*S. aureus*), which indicates that the presence of a biological microlens significantly enhances the upconversion fluorescence of *E. coli* and *S. aureus*. In addition, *S. aureus* and *E. coli* can be trapped and linked together, and their upconverted fluorescence signals can be simultaneously enhanced by approximately ~110. Moreover, Li et al. used living cells as biological lenses, demonstrating that cellular biological microlenses can also sense and enhance the fluorescence of particles with single-cell resolution [79]. The microlenses can also be manipulated in three dimensions by the light force generated by the optical tweezers. In 2020, using an optical tweezers system, Chen et al. moved $C_{10}H_7Br$ microlenses of different diameters above the CdSe@ZnS quantum dots with an emission wavelength of 550 nm [115]. The quantum dots were excited by the light of a mercury lamp filter. Under the microlens, the quantum dot fluorescence signal was sufficiently enhanced and detectable. By moving the microlens vertically along the Z axis, the brightest fluorescent spot in the field of view and the light intensity distribution corresponding to the dark field image were obtained, with a smaller diameter microlens boasting a strong signal enhancement (Figure 4c).

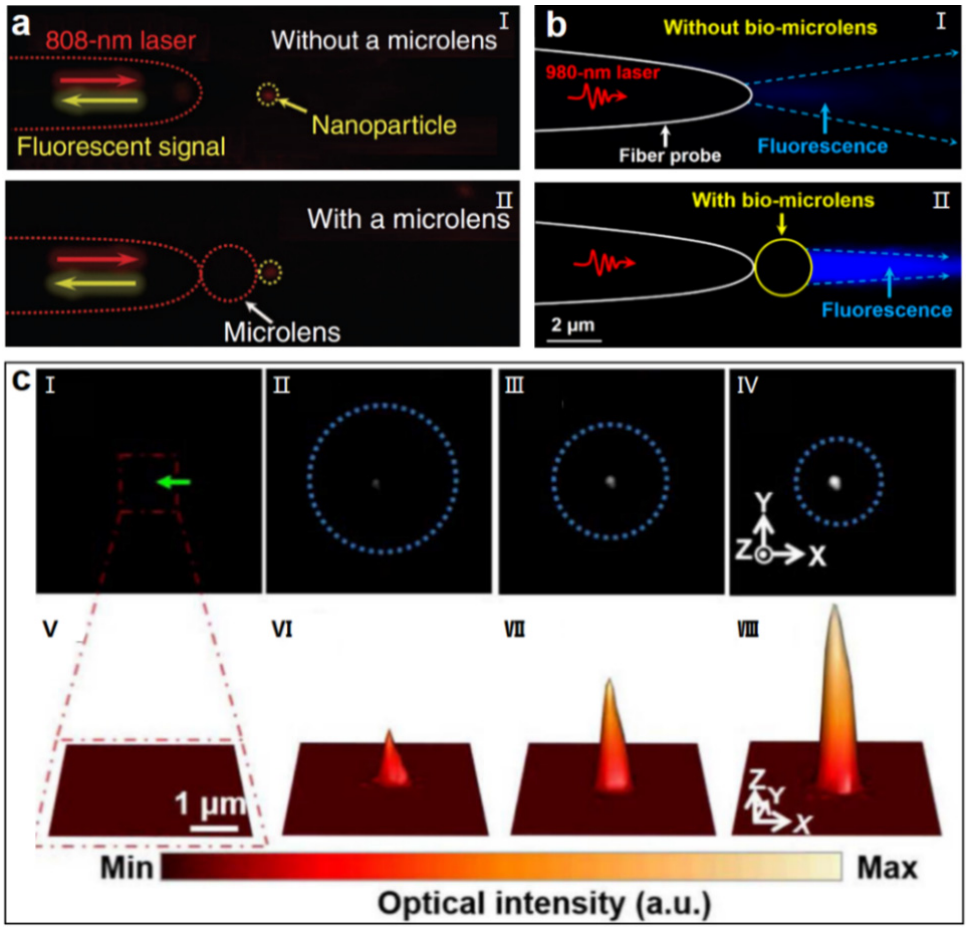

Figure 4. Fluorescence signal enhancement of microsphere superlenses. (**a**) Fluorescence signal images of the fiber without (I) and with (II) microlens for the sensing of individual nanoparticles; (**b**) Fluorescent image of the UCNP solution with fiber probe without (I) and with (II) biological microlens; (**c**) Fluorescence images of quantum dots with different diameters of $C_{10}H_7Br$ microlenses using optical tweezers.

3.2. Backscattering Signal Enhancement of Trapped Nano-Objects

When the highly focused beam generated by the microlens is irradiated on nanoparticles, the backscattering signal of the trapped nanoparticles can be significantly enhanced, thereby enhancing the sensing ability of the nanoparticles. It is beneficial to sense nanoparticles by analyzing the intensity and angular distribution of the enhanced backscattering from nanoparticles located in a photonic nanojet. In 2004, Chen et al. demonstrated through a two-dimensional numerical study that photonic nanojets can significantly enhance the backscattering of light by nanoparticles located within a nanojet [43]. Li et al. further proved enhanced backscattering of visible light by nanoparticles through a study of photonic nanojets [72]. Under light irradiation of different wavelengths, the backscattered signal of nanoparticles can be enhanced, whereas the enhanced backscattered power also varies, where dielectric microspheres act as microlenses to favor backscattered radiation [116]. Soon after, Yang et al. [117] experimentally verified for the first time that a photonic nanojet generated at visible wavelength can enhance the backscattering signal of nanoparticles. The photonic nanojet generated by $BaTiO_3$ microspheres with a diameter of 4.4 μm in the PDMS film can precisely locate and sense gold nanoparticle microspheres with diameters in the range of 50–100 nm.

As technology has evolved, there is considerable interest in high-resolution sensing systems that can trap and sense nano-objects and even single molecules in liquids. In 2015, researchers irradiated an array of melamine microspheres self-assembled in a microfluidic

channel using an illuminated light source from an optical microscope, and the resulting photonic nanojets sensed 50–400 nm diameter Au nanoparticles flowing in the channel [102]. As shown in Figure 5a,b, the backscattered light intensity of Au nanoparticles at 200 nm on the photonic nanojet is approximately 40 times stronger than the backscattered light intensity outside the photonic nanojet. The backscattering signal of trapped nanoparticles can be sensed more flexibly by fiber tweezers with microlenses because of the small size of nanoparticles and their susceptibility to Brownian motion in solution. Li et al. used fiber tweezers to trap TiO_2 microlenses at the tip of a fiber probe [109], and a single 85 nm fluorescent nanoparticle was trapped and sensed by a highly focused photonic nanojet generated by a microlens. In the process of trapping fluorescent nanoparticles, the backscatter signal is divided into three processes: before trapping the nanoparticles, trapping the nanoparticles, and releasing the nanoparticles. When the nanoparticles are trapped, the intensity of the backscatter signal is significantly enhanced (Figure 5c). In addition, plasmid DNA biomolecules with low refractive index, small volume, and irregular shape can be sensed using the device because the photonic nanojet generated by the microlenses can enhance the backscattering signal.

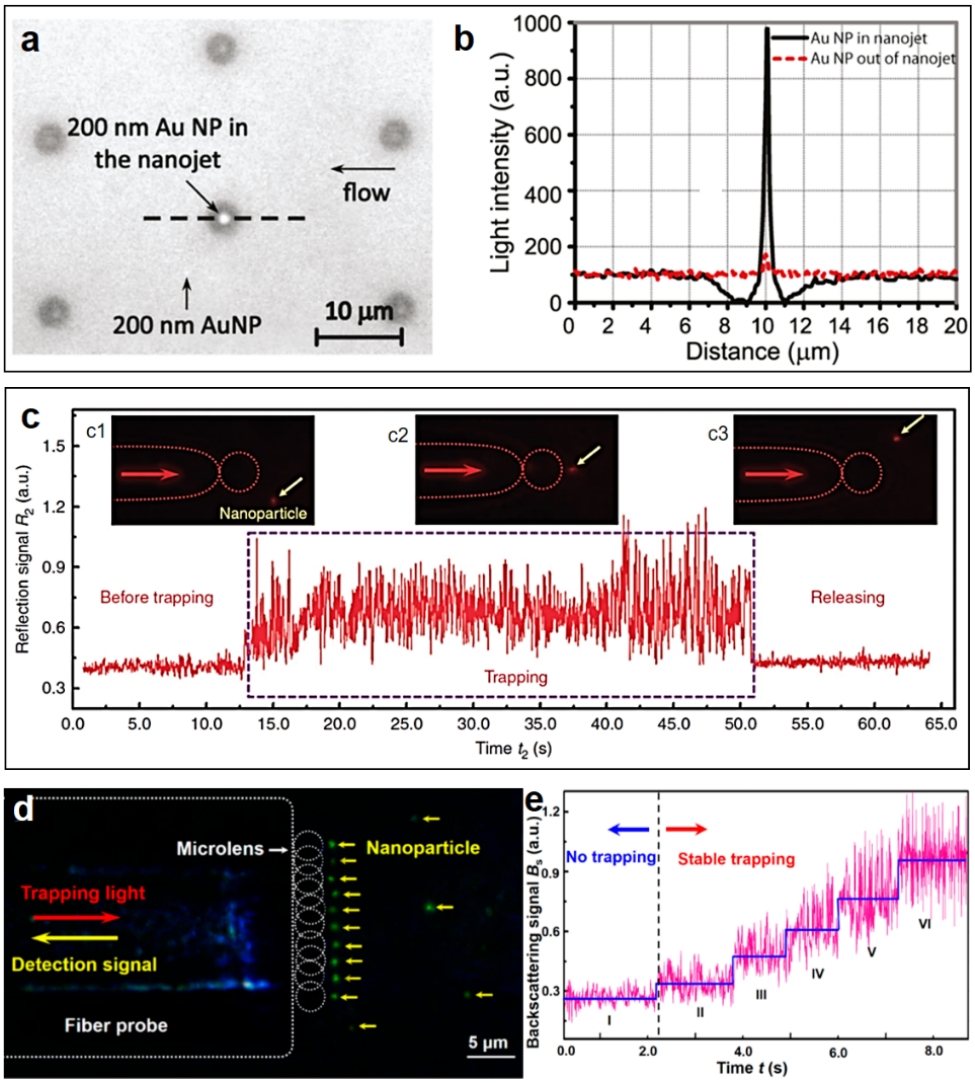

Figure 5. Backscattering signal enhancement of microlenses. (**a**) Two hundred nanometer diameter Au nanoparticles on a photonic nanojet; (**b**) Fluorescent image of UCNP solution with fiber probe without (I) and with (II) biological microlens; (**c**) Optical trapping of fluorescent nanoparticles by TiO_2 microlenses; (**d**) Optical images of fluorescent nanoparticles trapped by a microlens array; (**e**) Backscattering signals during trapping of multiple nanoparticles.

Next, Li's team assembled microsphere arrays on the end faces of fiber probes to trap and sense nanoparticles and subwavelength cells with high throughput, single nanoparticle resolution, and high selectivity [118]. As shown in Figure 5d,e, nanoparticles or cells were trapped using in-parallel photonic nanojet arrays, and their backscattered signals were sensing in real time with single-nanoparticle resolution, allowing for the detection of multiple nanoparticles and cells. To improve the sensitivity and biocompatibility of the detection, the team also used yeast as a biological microlens and trapped yeast using fiber tweezers to enhance the backscattering signal of *E. coli* chains [114], indicating prospects for single cell analysis and nanosensor applications.

3.3. Raman Signal Enhancement by Microsphere Superlens

Surface enhanced Raman scattering (SERS) is widely used in the analysis and sensing of materials. The Raman enhancement method of a photonic nanojet based on microspheres is a simple and reliable method. In 2007, Yi's team enhanced the Raman peak of Si by self-assembling SiO_2 microspheres on a silicon substrate because of the photonic nanojet effect produced by microspheres [119]. Transparent medium microspheres focus light to the finite size of sub-diffraction and focus visible light strongly in the photonic nanojet. As a result, the Raman signal of the measured object can be enhanced using microspheres [120]. In 2010, Du et al. demonstrated that a single dielectric microsphere can also enhance the Raman signal and that the enhancement is related to the size of the microsphere [77]. As shown in Figure 6a, a Raman peak was detected at 520 cm^{-1} when a PS microsphere with a refractive index of 1.59 was placed on the surface of a single crystal Si, while the Raman spectrum of only the PS microsphere had no peak at the same wavelength. This indicates that the characteristic peak of Si is significantly enhanced in the presence of a microlens.

In addition, a self-assembled high refractive index droplet microlens can enhance the Raman signal of Si wafers [115]. For bare silicon wafers or wafer regions without droplet microlenses, the detected Raman signal was very weak. When a suspension of the droplet microlens is placed on the silicon wafer, the microlens adheres to the silicon wafer surface by gravity, and the Raman signal of the silicon wafer is fully enhanced. The enhancement of the Raman signal is also different for droplet microlenses with different diameters (Figure 6b). The combination of a microsphere superlens and a solid film can also enhance the detection of Raman signals. Xing et al. immersed a monolayer of highly refractive $BaTiO_3$ microspheres into PDMS membranes and then transferred them to the sample surface for Raman detection [121]. As shown in Figure 6c,d, flexible microspheres embedded in thin films can enhance the Raman signal of one-dimensional carbon nanotubes and two-dimensional graphene. Furthermore, crystal violet molecules and Sudan I molecules can be tracked and sensed in aqueous solutions at a concentration of 10^{-7} M by coupling the flexible microsphere embedded film with silver nanoparticles or silver films. The flexible microsphere embedded film increases the SERS of the sample by 10 times and increases the sensing limit by at least an order of magnitude. To sense Raman signals more flexibly, microlenses can be combined with fiber probes [122]. Laser enhancement was achieved by focusing the incident laser on the silicon wafer surface through the microsphere on the probe, and it was observed experimentally that the tapered fiber could not effectively enhance the Raman scattering signal, and the Raman signal increased with the distance from the Raman microscope focal length.

All of the above Raman enhancement methods use fixed microspheres to enhance localized areas underneath them for single point acquisition of the sample. Recently, some researchers achieved Raman mapping enhancement of samples using microspheres [123]. As shown in Figure 6e,f, 5 μm SiO_2 microspheres attached to two vertical optical fibers were placed on a polysilicon substrate. As the sample is mapped, the microsphere stays under the laser beam of the objective lens and at the position of the microscope objective while the substrate moves below it. Therefore, all points of the image can be enhanced, and the signal enhancement at each point is $\times 4$.

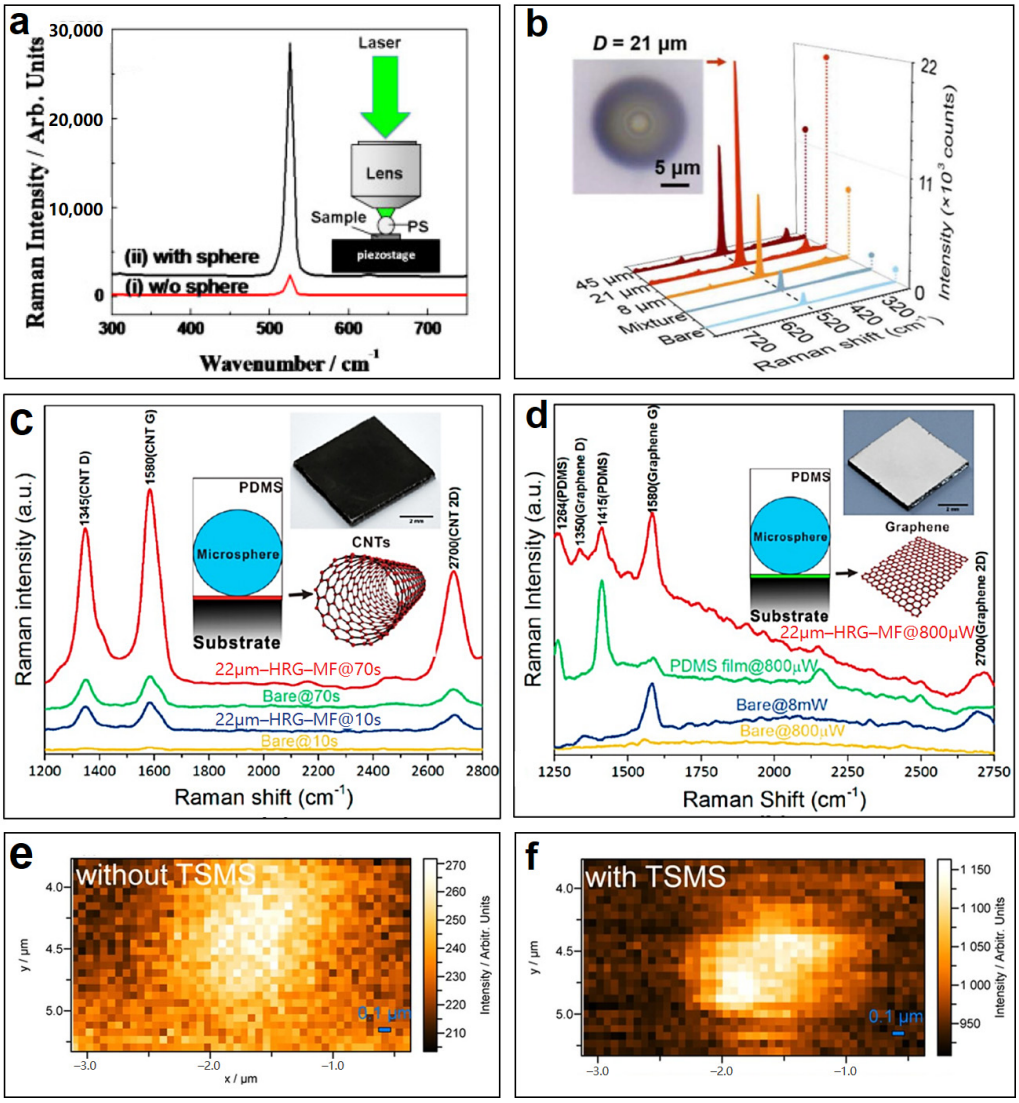

Figure 6. Raman enhancement of the microsphere lens. (**a**) Raman spectra of a Si wafer without PS microsphere (i) and with PS microsphere (ii); (**b**) Raman scattering intensity of different diameters of $C_{10}H_7Br$ microlenses on silicon wafers; Raman spectra of microspheres with and without high refractive index on (**c**) 1D carbon nanotubes and (**d**) 2D graphene; Raman mapping (**e**) with and (**f**) without microlens.

4. Super-Resolution Imaging by Photonic Nanojets

4.1. Optical Imaging of Nanostructures with Movable Microspheres

Microsphere lenses can be prepared by a variety of materials and methods [124–127], allowing high-resolution optical imaging of solid nanostructures at very low light intensities. As shown in Figure 7a, Wang et al. used SiO_2 microspheres with a diameter of 4.74 μm to image a gold-plated porous anodic aluminum oxide film with a diameter of 50 nm under white light conditions [44]. This method achieves real-time, label-free super-resolution imaging under white light conditions. Darafsheh et al. [63] immersed 5 μm $BaTiO_3$ microspheres in a liquid and achieved imaging of nanoplasmonic samples with a gap of 50–60 nm under irradiation at a wavelength of 405 nm (Figure 7b). In addition, super-resolution imaging of 250 nm metal fringes was achieved by the nano-scale flat spherical microlens prepared by chemically assembling the organic molecule hydroquinone from bottom to top [118]. Lee et al. used TiO_2 with a diameter of 60 μm and a refractive index of 2.2 to wrap ZnO, and the structure of 100–200 nm on Blu-ray discs was observed using a standard optical microscope [128]. Furthermore, Fan et al. [129] compactly stacked 45 nm

anatase TiO_2 nanoparticles with a transparent refractive index of 2.55 using a solid-phase fluidic method. When a superlens comprising TiO_2 was located on a semiconductor wafer containing a parallel line pattern or a dotted line pattern, an image with a pitch of 60 nm and a complex structure of 50 nm was observed (Figure 7c). Dhama et al. [130] theoretically and experimentally demonstrated that a superlens comprising TiO_2 nanoparticles consistently outperformed $BaTiO_3$ microspheres in terms of imaging contrast, sharpness, field of view, and resolution because the tightly stacked 15 nm anatase TiO_2 nanoparticle composites have tiny air gaps between the particles, causing a dense scattering medium. Moreover, TiO_2 has almost no visible wavelength of energy dissipation. As a result, this near-field coupling effect between adjacent nanoparticles can be effectively propagated through the medium over long distances. The nanoparticle-synthesized medium will have the unusual ability to transform far-field illumination into large-area, nanoscale fading-wave illumination focused on the surface of an object in the near-field region. In addition, Wang et al. [131] used cylindrical spider silk under a traditional white light microscope with a wavelength of 600 nm to clearly distinguish 100 nm objects. This is due to the near-field interaction between the spider silk and the underlying nano-object, which causes the high spatial frequency evanescent wave at the surface boundary to be converted into a propagating wave. However, under dry conditions, super-resolution imaging cannot be achieved with spider silk. When isopropanol is used to fill regional gaps, the object can be super-resolution imaged due to the capillary binding force that occurs in the interface area. When the incident angle changes, the distance between the object and the lens also changes, so that the magnification factor can be adjusted.

To further increase the field of view of the microspheres in super-resolution imaging, large-area imaging can be achieved at a controllable position. Li et al. achieved stable and controllable image scanning of samples using chemical dynamics to drive the microsphere lens [132]. In addition, various attempts have been made to improve the field of view of microspheres in super-resolution imaging and achieve large-area imaging in a controllable position [133,134]. Krivitsky et al. achieved sample imaging of gold split squares deposited on silicon substrates with 73 nm gaps using a micropipette for accurate positioning between the squares [135], as shown in Figure 7d. The microsphere can also be combined with the cantilever of an atomic force microscope. The position of the microsphere can be changed by moving the cantilever, so that near-field information of the target position can be collected, and super-resolution images of any sample area can be obtained [136]. As shown in Figure 7e, the microspheres on the cantilever are used to approach the sample to realize imaging of the disc with a spacing of 80 nm. Moreover, the fiber probe can also act as a cantilever to improve the flexibility of imaging, using fiber tweezers to trap cells and scan the characters etched on the silicon substrate at a rate of ~20 μm/s [79], as shown in Figure 7f. Additionally, a 2 × 2 $C_{10}H_7Br$ droplet microlens array was assembled using optical tweezers [115] and the assembled droplet microlens was transferred to the polystyrene nanoparticle surface of the stack, where the contour of the nanoparticle became apparent in the field of view of the microscope (Figure 7g). Allen et al. [137] used high refractive index (n = 2) $BaTiO_3$ microspheres embedded in PDMS films to achieve large area imaging of 60 nm Au dimer spacing and 15 nm butterfly junction arrays. Zhang et al. [138] used $BaTiO_3$ microspheres embedded in PDMS films to image the streak structure on the surface of a Blu-ray disc (Figure 7h). Furthermore, through the dynamic scanning imaging mode of the microlens array and the superimposed reconstruction mode of the random microlens array area imaging, a 900 μm^2 surface image stitched by 210 images was realized (Figure 7i), which can reduce the number of images needed, improve imaging efficiency, and improve the observation range.

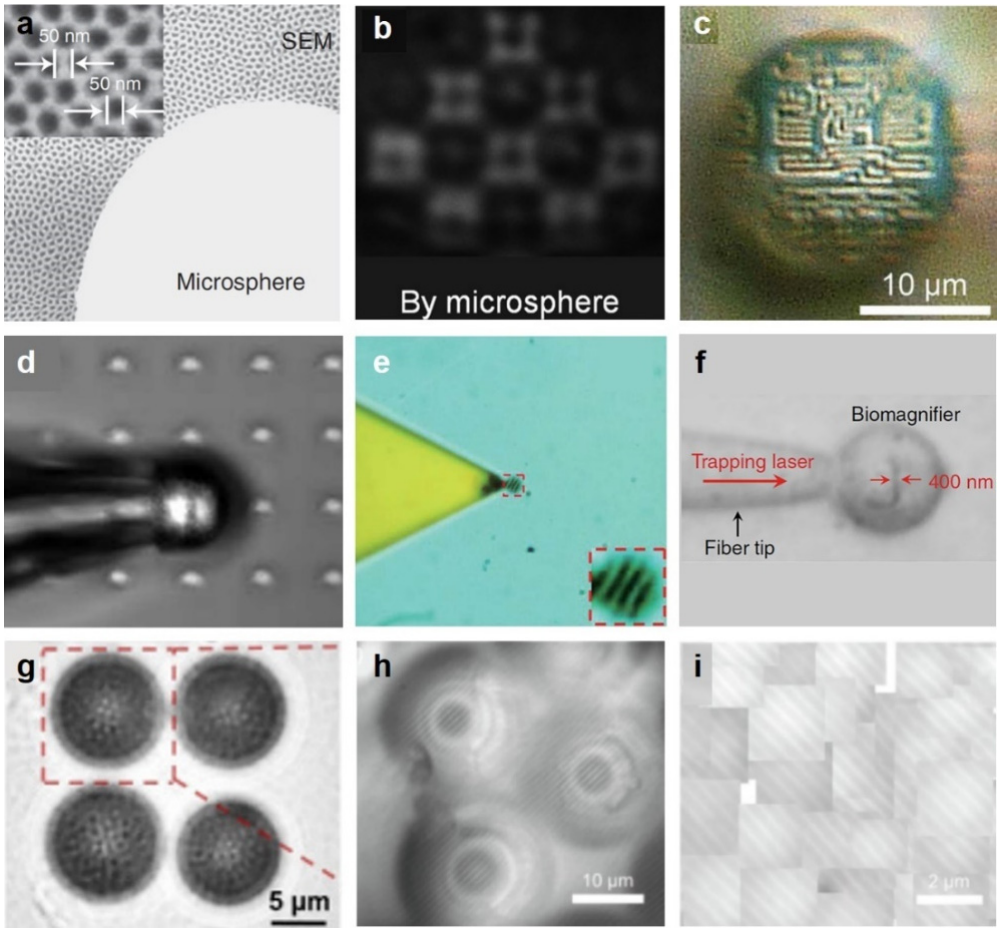

Figure 7. Optical imaging of nanostructures with microspheres. (**a**) SiO_2 microspheres on gold-plated porous anodic aluminum oxide film; (**b**) $BaTiO_3$ microspheres on nano-plasma samples with a gap of 50–60 nm; (**c**) TiO_2 microsphere superlenses on 60 nm wafers; (**d**) Magnified image of gold splitting square nanostructures imaged using microspheres combined with micropipettes; (**e**) Magnified image of a microsphere combined with an AFM cantilever against a DVD; (**f**) Optical images of nanopatterns trapped on the fiber of a biomagnifier; (**g**) Optical images of PS nanoparticles by a 2 × 2 microlens array; (**h**) Large-area imaging of Blu-ray discs by $BaTiO_3$ microlenses; (**i**) The Blu-ray disc surface recorded using the random microlens array area imaging superimposed reconstruction mode.

4.2. Super-Resolution Imaging of Living Cells by Photonic Nanojets

The combination of microsphere superlenses and an optical imaging device for biological imaging and analysis has been confirmed by many researchers. Fluorescence microscopy is generally used to observe cell structure and image bacteria, but the observation of specific biological organelles in vitro requires staining [139]. In 2014, Yang et al. [140] combined fluorescence microscopy with $BaTiO_3$ microspheres with a refractive index n = 1.92 and a diameter of 60 μm to image several different organelles in the alpha mouse liver 12 (AML12) cell line. As shown in Figure 8a, the traditional optical microscope can be used to identify the existence of centrioles, but it cannot observe their fine structure. The ring structure and γ-tubulin fluorescence labeling of the two centrioles was observed when the microsphere was placed above the centrosome, and even the junction of the two centrioles was identified. The mitochondria were then stained, and the fluorescence images of mitochondria were obtained using traditional light microscopy and microspheres. The complex shapes of the mitochondria were distinguished using $BaTiO_3$ microspheres. The influence of liquid evaporation on the imaging effect can be reduced by embedding the microspheres in transparent film and imaging with an inverted microscope. Darafsheh et al. obtained conventional fluorescence micrographs of cells under a fluorescence imaging mode by

immersing 130 μm $BaTiO_3$ microspheres in PDMS films and placing them on the specimen under excitation at 365 nm [64]. At an excitation of 594 nm, the $BaTiO_3$ microspheres act as an auxiliary microlens to form a magnified virtual image below the sample surface. The red lesions of proton beam induced double-stranded DNA breaks were observed through the objective lens (Figure 8b).

In addition, the super-resolution imaging of certain organisms can be performed without fluorescent labeling. Li et al. used $BaTiO_3$ microspheres with a refractive index of 1.9 and diameter of 100 μm to image adenovirus at 75 nm under white light without fluorescent labeling or staining [59]. When $BaTiO_3$ microspheres were placed on the virus, the adenovirus could not be distinguished using a low magnification objective. When passed through a high-magnification objective, the microsphere converted the evanescent wave in the near field into an amplified extended wave in the far field through a frustrated total internal reflection mechanism, and individual adenoviruses were resolved and imaged below the sample surface (Figure 8c). The focusing of light by the microspheres forms a nanojet, which transmits the converted propagating waves to the space outside the sphere, which plays an important role in enhancing the image contrast. Furthermore, Chernomyrdin et al. used a method of the terahertz solid immersion microscope to focus electromagnetic waves to the evanescent field volume through a lens, thereby reducing the size of the terahertz beam caustics [141]. When articular hyaline cartilage of male sheep is placed on the scanning window of the system, the tissue ellipsoid of sub-wavelength diameter can be distinguished.

The optical imaging of subcellular structures is generally achieved by the combination of a microsphere lens and microscope. However, trapping the microlens with fiber tweezers can magnify and image any position of the biological sample in real time. As shown in Figure 8d, it is difficult to distinguish the bilayer structure of the fibrous cytoskeleton and cell membrane in the cell under an ordinary light microscope, and yet, after trapping the cell microlens with fiber tweezers and placing it above the epithelial cells, the bilayer structure of the fibrous cytoskeleton and cell membrane were clearly observed by enhancing the interaction between light and matter through the interference of incident and reflected light [79]. At the same time, Li et al. performed a numerical simulation analysis on the semi-immersed microlens above the mirror and obtained the focused photonic nanojet of the microlens. The theoretical imaging resolution is 85 nm, which is slightly smaller than the experimental resolution. This deviation is mainly due to the geometric configuration and refractive index of the cell microlens is defined as completely symmetrical and uniform in the simulation. In addition, Wang et al. proposed the use of atomic force microscopy in combination with microlenses to achieve large-area observations of living cell morphology or submembrane structures at sub-diffraction limited resolution [142]. As Figure 8e shows a fluorescent picture of C2C12 cells, the actin filaments in the cells can be clearly observed by moving the 56 μm diameter $BaTiO_3$ microspheres to the cell surface with the cantilever of an AFM, which is an important step for real-time monitoring of the status of a cell.

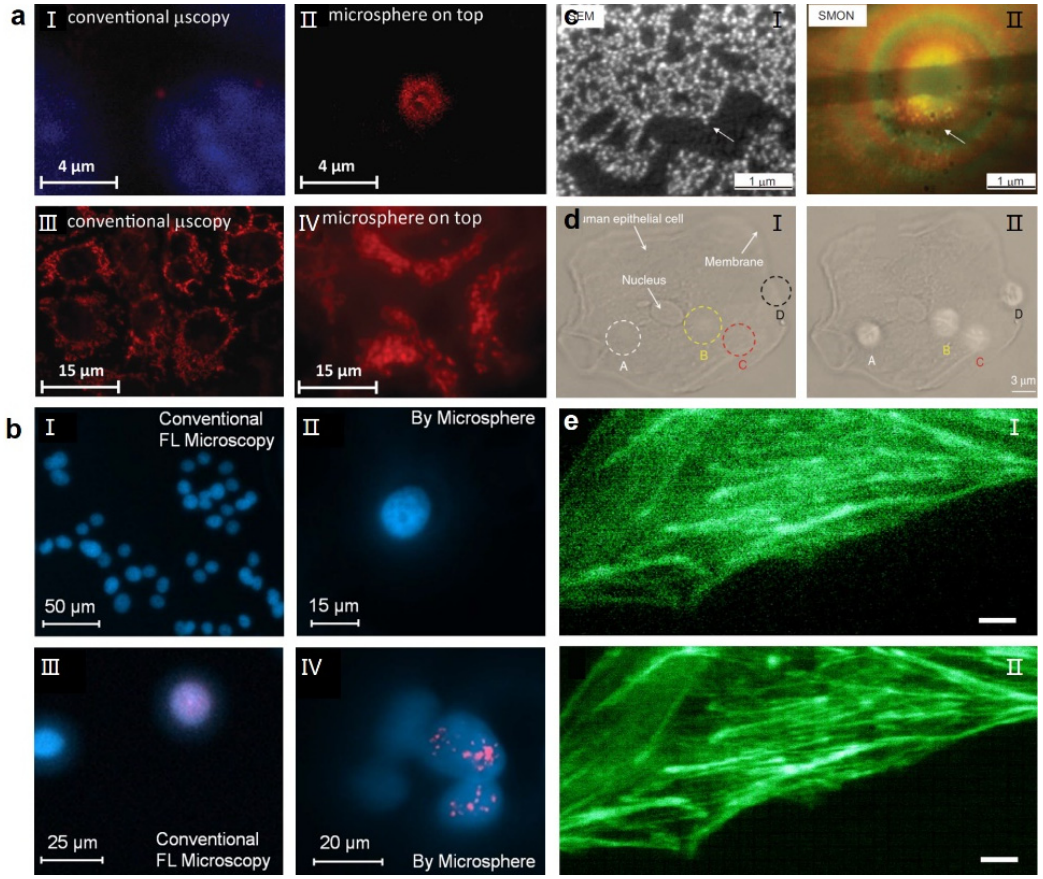

Figure 8. Super-resolution imaging of organisms. (**a**) Imaging of centrioles (I–II) and mitochondria (III–IV) of mouse hepatocyte lineage cells using conventional fluorescence microscopy and microsphere superlenses; (**b**) Optical images of cells without (I) and with (II) a microlens, and fluorescence images of cell nuclear double-stranded DNA imaging without a microlens (III) and with a microsphere superlens (IV); (**c**) SEM images of adenovirus by $BaTiO_3$ microspheres under white light (I) and imaging under $BaTiO_3$ (II).; (**d**) Imaging of the bilayer structure of the fibrous cytoskeleton and cell membrane without a microlens (I) and with a cellular lens (II); (**e**) Fluorescence imaging of C2C12 cells (I) and enhanced images with 56 μm diameter microsphere superlenses (II).

5. Conclusions and Outlook

This review systematically describes the application and progress of microsphere lenses in nano-optical trapping, sensing, and imaging from the types and principles of microsphere lenses. Thanks to the advantages of simple preparation, microsphere lenses provide a simple method for super-resolution imaging of biological samples and sensing of tiny particles, with potential value in biomedicine, microfluidics and nanophotonics. For another, microspheres can be combined with optical fibers, optical tweezers, and other tools to improve flexibility. Therefore, microspheres are expected to be constructed as photonic devices for biomedical imaging and real-time monitoring of samples, providing more promising technologies for biophotonics, nanophotonics, and biomedicine.

Most of the optical sensing and imaging based on microlenses are performed in vitro. However, these in vitro conditions cannot fully reflect the biological environment and conditions in vivo. Because the microlens is implantable, it has broad application prospects in in vivo nanomanipulation and biological detection. In addition, optical tweezers or optical traps provide a unique method of manipulating and controlling biological objects both in vivo and in vitro. The strong laser of light capture is prone to optical damage, which limits the exposure time of the captured sample. The photonic nanojet generated by the microlens may overcome optical opticution and allow the optical trapping of living cells to be widely implemented.

Author Contributions: Conceptualization, A.W.; writing—original draft preparation, H.L., W.S., and Y.Z.; writing—review and editing; A.W., Q.C. and H.L. All authors have read and agreed to the published version of the manuscript.

Funding: This research was funded by the Fundamental Research Funds for the Central Universities, grant number 21619321.

Institutional Review Board Statement: Not applicable.

Informed Consent Statement: Not applicable.

Data Availability Statement: The data that support the findings of this study and available from the corresponding author upon reasonable request.

Conflicts of Interest: The authors declare no conflict of interest.

References

1. Gu, M.; Bao, H.; Gan, X.; Stokes, N.; Wu, J. Tweezing and manipulating micro-and nanoparticles by optical nonlinear endoscopy. *Light Sci. Appl.* **2014**, *3*, e126. [CrossRef]
2. Gautam, R.; Xiang, Y.; Lamstein, J.; Liang, Y.; Bezryadina, A.; Liang, G.; Hansson, T.; Wetzel, B.; Preece, D.; White, A.; et al. Optical force-induced nonlinearity and self-guiding of light in human red blood cell suspensions. *Light Sci. Appl.* **2019**, *8*, 31. [CrossRef] [PubMed]
3. Bezryadina, A.S.; Preece, D.C.; Chen, J.C.; Chen, Z. Optical disassembly of cellular clusters by tunable 'tug-of-war' tweezers. *Light Sci. Appl.* **2016**, *5*, e16158. [CrossRef] [PubMed]
4. Singh, B.K.; Nagar, H.; Roichman, Y.; Arie, A. Particle manipulation beyond the diffraction limit using structured super-oscillating light beams. *Light Sci. Appl.* **2017**, *6*, e17050. [CrossRef] [PubMed]
5. Lepage, D.; Jiménez, A.; Beauvais, J.; Dubowski, J.J. Real-time detection of influenza a virus using semiconductor nanophotonics. *Light Sci. Appl.* **2013**, *2*, e62. [CrossRef]
6. Lee, S.; Kwon, O.; Jeon, M.; Song, J.; Shin, S.; Kim, H.; Jo, M.; Rim, T.; Dosh, J.; Kim, S.; et al. Super-resolution visible photoactivated atomic force microscopy. *Light Sci. Appl.* **2017**, *6*, e17080. [CrossRef]
7. Lombardini, A.; Mytskaniuk, V.; Sivankutty, S.; Andresen, E.R.; Chen, X.; Wenger, J.; Fabert, M.; Joly, N.; Louradour, F.; Kudlinski, A.; et al. High-resolution multimodal flexible coherent Raman endoscope. *Light Sci. Appl.* **2018**, *7*, 10. [CrossRef]
8. Petsch, S.; Schuhladen, S.; Dreesen, L.; Zappe, H. The engineered eyeball, a tunable imaging system using soft-matter micro-optics. *Light Sci. Appl.* **2016**, *5*, e16068. [CrossRef] [PubMed]
9. Zhang, W.; Zappe, H.; Seifert, A. Wafer-scale fabricated thermo-pneumatically tunable microlenses. *Light Sci. Appl.* **2014**, *3*, e145. [CrossRef]
10. Kim, K.; Jang, K.W.; Ryu, J.K.; Jeong, K.H. Biologically inspired ultrathin arrayed camera for high-contrast and high-resolution imaging. *Light Sci. Appl.* **2020**, *9*, 28. [CrossRef] [PubMed]
11. Li, Y.; Xin, H.; Zhang, Y.; Li, B. Optical fiber technologies for nanomanipulation and biodetection: A review. *J. Lightwave Technol.* **2021**, *39*, 251–262. [CrossRef]
12. Lei, H.; Zhang, Y.; Li, X.; Li, B. Photophoretic assembly and migration of dielectric particles and Escherichia coli in liquids using a subwavelength diameter optical fiber. *Lab Chip* **2011**, *11*, 2241–2246. [CrossRef]
13. Pan, T.; Lu, D.; Xin, H.; Li, B. Biophotonic probes for bio-detection and imaging. *Light Sci. Appl.* **2021**, *10*, 124. [CrossRef] [PubMed]
14. Su, J.; Goldberg, A.F.G.; Stoltz, B.M. Label-free detection of single nanoparticles and biological molecules using microtoroid optical resonators. *Light Sci. Appl.* **2016**, *5*, e16001. [CrossRef]
15. Yu, X.C.; Zhi, Y.; Tang, S.J.; Li, B.B.; Gong, Q.; Qiu, C.W.; Xiao, Y.F. Optically sizing single atmospheric particulates with a 10-nm resolution using a strong evanescent field. *Light Sci. Appl.* **2018**, *7*, 18003. [CrossRef] [PubMed]
16. Abbe, E. Beiträge zur Theorie des Mikroskops und der mikroskopischen Wahrnehmung. *Archiv für mikroskopische Anatomie* **1873**, *9*, 413–468. [CrossRef]
17. Hao, X.; Kuang, C.; Gu, Z.; Wang, Y.; Li, S.; Ku, Y.; Li, Y.; Ge, J.; Liu, X. From microscopy to nanoscopy via visible light. *Light Sci. Appl.* **2013**, *2*, e108. [CrossRef]
18. Yang, X.; Xie, H.; Alonas, E.; Liu, Y.; Chen, X.; Santangelo, P.J.; Ren, Q.; Xi, P.; Jin, D. Mirror-enhanced super-resolution microscopy. *Light Sci. Appl.* **2016**, *5*, e16134. [CrossRef] [PubMed]
19. Xiong, H.; Qian, N.; Miao, Y.; Zhao, Z.; Chen, C.; Min, W. Super-resolution vibrational microscopy by stimulated Raman excited fluorescence. *Light Sci. Appl.* **2021**, *10*, 87. [CrossRef]
20. Gao, D.; Ding, W.; Nieto-Vesperinas, M.; Ding, X.; Rahman, M.; Zhang, T.; Lim, C.; Qiu, C.W. Optical manipulation from the microscale to the nanoscale: Fundamentals, advances and prospects. *Light Sci. Appl.* **2017**, *6*, e17039. [CrossRef]

21. Yuan, G.H.; Rogers, E.T.F.; Zheludev, N.I. Achromatic super-oscillatory lenses with sub-wavelength focusing. *Light Sci. Appl.* **2017**, *6*, e17036. [CrossRef]
22. Eberle, A.L.; Mikula, S.; Schalek, R.; Lichtman, J.; Tate, M.K.; Zeidler, D. High-resolution, high-throughput imaging with a multibeam scanning electron microscope. *J. Microsc.* **2015**, *259*, 114–120. [CrossRef]
23. Browning, N.D.; Chisholm, M.; Pennycook, S.J. Atomic-resolution chemical analysis using a scanning transmission electron microscope. *Nature* **1993**, *366*, 143–146. [CrossRef]
24. Huang, B.; Bates, M.; Zhuang, X. Super-resolution fluorescence microscopy. *Annual Rev. Biochem.* **2009**, *78*, 993–1016. [CrossRef]
25. Dong, D.; Huang, X.; Li, L.; Mao, H.; Mo, Y.; Zhang, G.; Zhang, Z.; Shen, J.; Liu, W.; Wu, Z.; et al. Super-resolution fluorescence-assisted diffraction computational tomography reveals the three-dimensional landscape of the cellular organelle interactome. *Light Sci. Appl.* **2020**, *9*, 11. [CrossRef]
26. Ash, E.A.; Nicholls, G. Super-resolution aperture scanning microscope. *Nature* **1972**, *237*, 510–512. [CrossRef]
27. Pohl, D.W.; Denk, W.; Lanz, M. Optical stethoscopy: Image recording with resolution $\lambda/20$. *Appl. Phys. Lett.* **1984**, *44*, 651–653. [CrossRef]
28. Hosaka, N.; Saiki, T. Near-field fluorescence imaging of single molecules with a resolution in the range of 10 nm. *J. Microsc.* **2001**, *202*, 362–364. [CrossRef]
29. Pendry, J.B. Negative refraction makes a perfect lens. *Phys. Rev. Lett.* **2000**, *85*, 3966. [CrossRef]
30. Fang, N.; Lee, H.; Sun, C.; Zhang, X. Sub–diffraction-limited optical imaging with a silver superlens. *Science* **2005**, *308*, 534–537. [CrossRef]
31. Huang, S.; Wang, H.; Ding, K.H.; Tsang, L. Subwavelength imaging enhancement through a three-dimensional plasmon superlens with rough surface. *Opt. Lett.* **2012**, *37*, 1295–1297. [CrossRef]
32. Wang, C.; Zhang, W.; Zhao, Z.; Wang, Y.; Gao, P.; Luo, Y.; Luo, X. Plasmonic structures, materials and lenses for optical lithography beyond the diffraction limit: A review. *Micromachines* **2016**, *7*, 118. [CrossRef]
33. Barnes, W.L.; Dereux, A.; Ebbesen, T.W. Surface plasmon subwavelength optics. *Nature* **2003**, *424*, 824–830. [CrossRef]
34. Ivinskaya, A.; Petrov, M.I.; Bogdanov, A.A.; Shishkin, I.; Ginzburg, P.; Shalin, A.S. Plasmon-assisted optical trapping and anti-trapping. *Light Sci. Appl.* **2017**, *6*, e16258. [CrossRef]
35. Crozier, K.B. Quo vadis, plasmonic optical tweezers? *Light Sci. Appl.* **2019**, *8*, 35. [CrossRef]
36. Mestres, P.; Berthelot, J.; Aćimović, S.S.; Quidant, R. Unraveling the optomechanical nature of plasmonic trapping. *Light Sci. Appl.* **2016**, *5*, e16092. [CrossRef]
37. Li, Y.; Svitelskiy, O.V.; Maslov, A.V.; Carnegie, D.; Rafailov, E.; Astratov, V.N. Giant resonant light forces in microspherical photonics. *Light Sci. Appl.* **2013**, *2*, e64. [CrossRef]
38. Zhang, Y.; Min, C.; Dou, X.; Wang, X.; Urbach, H.P.; Somekh, M.G.; Yuan, X. Plasmonic tweezers: For nanoscale optical trapping and beyond. *Light Sci. Appl.* **2021**, *10*, 59. [CrossRef]
39. Bykov, D.S.; Xie, S.; Zeltner, R.; Machnev, A.; Wong, G.K.; Euser, T.G.; Russell, P.S.J. Long-range optical trapping and binding of microparticles in hollow-core photonic crystal fibre. *Light Sci. Appl.* **2018**, *7*, 22. [CrossRef]
40. Upputuri, P.K.; Pramanik, M. Microsphere-aided optical microscopy and its applications for super-resolution imaging. *Opt. Commun.* **2017**, *404*, 32–41. [CrossRef]
41. Toropov, N.; Cabello, G.; Serrano, M.P.; Gutha, R.R.; Rafti, M.; Vollmer, F. Review of biosensing with whispering-gallery mode lasers. *Light Sci. Appl.* **2021**, *10*, 42. [CrossRef]
42. Zhao, X.; Sun, Y.; Bu, J.; Zhu, S.; Yuan, X.C. Microlens-array-enabled on-chip optical trapping and sorting. *Appl. Opt.* **2011**, *50*, 318–322. [CrossRef]
43. Chen, Z.; Taflove, A.; Backman, V. Photonic nanojet enhancement of backscattering of light by nanoparticles: A potential novel visible-light ultramicroscopy technique. *Opt. Express* **2004**, *12*, 1214–1220. [CrossRef]
44. Wang, Z.; Guo, W.; Li, L.; Luk'Yanchuk, B.; Khan, A.; Liu, Z.; Chen, Z.; Hong, M. Optical virtual imaging at 50 nm lateral resolution with a white-light nanoscope. *Nat. Commun.* **2011**, *2*, 218. [CrossRef]
45. Ferrand, P.; Wenger, J.; Devilez, A.; Pianta, M.; Stout, B.; Bonod, N.; Popov, E.; Rigneault, H. Direct imaging of photonic nanojets. *Opt. Express* **2008**, *16*, 6930–6940. [CrossRef]
46. Yousefi, M.; Scharf, T.; Rossi, M. Photonic nanojet generation under converging and diverging beams. *J. Opt. Soc. Am. B* **2021**, *38*, 317–326. [CrossRef]
47. Han, L.; Han, Y.; Gouesbet, G.; Wang, J.; Gréhan, G. Photonic jet generated by spheroidal particle with Gaussian-beam illumination. *J. Opt. Soc. Am. B* **2014**, *31*, 1476–1483. [CrossRef]
48. Luk'yanchuk, B.S.; Paniagua-Domínguez, R.; Minin, I.; Minin, O.; Wang, Z. Refractive index less than two: Photonic nanojets yesterday, today and tomorrow. *Opt. Mater. Express* **2017**, *7*, 1820–1847. [CrossRef]
49. Darafsheh, A.; Bollinger, D. Systematic study of the characteristics of the photonic nanojets formed by dielectric microcylinders. *Opt. Commun.* **2017**, *402*, 270–275. [CrossRef]
50. Gu, G.; Song, J.; Chen, M.; Peng, X.; Liang, H.; Qu, J. Single nanoparticle detection using a photonic nanojet. *Nanoscale* **2018**, *10*, 14182–14189. [CrossRef]

51. Tsai, M.C.; Tsai, T.L.; Shieh, D.B.; Chiu, H.T.; Lee, C.Y. Detecting HER2 on cancer cells by TiO_2 spheres Mie scattering. *Anal. Chem.* **2009**, *81*, 7590–7596. [CrossRef]
52. Darafsheh, A. Photonic nanojets and their applications. *J. Phys. Photon.* **2021**, *3*, 022001. [CrossRef]
53. Lecler, S.; Haacke, S.; Lecong, N.; Crégut, O.; Rehspringer, J.L.; Hirlimann, C. Photonic jet driven non-linear optics: Example of two-photon fluorescence enhancement by dielectric microspheres. *Opt. Express* **2007**, *15*, 4935–4942. [CrossRef]
54. Biccari, F.; Hamilton, T.; Ristori, A.; Sanguinetti, S.; Bietti, S.; Gurioli, M.; Mohseni, H. Quantum dots luminescence collection enhancement and nanoscopy by dielectric microspheres. *Part. Part. Syst. Charact.* **2020**, *37*, 1900431. [CrossRef]
55. Das, G.M.; Ringne, A.B.; Dantham, V.R.; Easwaran, R.K.; Laha, R. Numerical investigations on photonic nanojet mediated surface enhanced Raman scattering and fluorescence techniques. *Opt. Express* **2017**, *25*, 19822–19831. [CrossRef]
56. Ren, Y.X.; Zeng, X.; Zhou, L.M.; Kong, C.; Mao, H.; Qiu, C.W.; Tsia, K.K.; Wong, K.K. Photonic nanojet mediated backaction of dielectric microparticles. *ACS Photonics* **2020**, *7*, 1483–1490. [CrossRef]
57. Sun, S.; Li, M.; Du, Q.; Png, C.E.; Bai, P. Metal–dielectric hybrid dimer nanoantenna: Coupling between surface plasmons and dielectric resonances for fluorescence enhancement. *J. Phys. Chem. C* **2017**, *121*, 12871–12884. [CrossRef]
58. Migliozzi, D.; Gijs, M.A.; Huszka, G. Microsphere-mediated optical contrast tuning for designing imaging systems with adjustable resolution gain. *Sci. Reports* **2018**, *8*, 15211. [CrossRef]
59. Li, L.; Guo, W.; Yan, Y.; Lee, S.; Wang, T. Label-free super-resolution imaging of adenoviruses by submerged microsphere optical nanoscopy. *Light Sci. Appl.* **2013**, *2*, e104. [CrossRef]
60. Hao, X.; Kuang, C.; Liu, X.; Zhang, H.; Li, Y. Microsphere based microscope with optical super-resolution capability. *Appl. Phys. Lett.* **2011**, *99*, 203102. [CrossRef]
61. Darafsheh, A.; Walsh, G.F.; Dal Negro, L.; Astratov, V.N. Optical super-resolution by high-index liquid-immersed microspheres. *Appl. Phys. Lett.* **2012**, *101*, 141128. [CrossRef]
62. Darafsheh, A.; Limberopoulos, N.I.; Derov, J.S.; Walker, D.E., Jr.; Durska, M.; Krizhanovskii, D.N.; Whittaker, D.M.; Astratov, V.N. Optical microscopy with super-resolution by liquid-immersed high-index microspheres. *Proc. SPIE* **2013**, *8594*, 85940C. [CrossRef]
63. Darafsheh, A.; Limberopoulos, N.I.; Derov, J.S.; Walker, D.E., Jr.; Astratov, V.N. Advantages of microsphere-assisted super-resolution imaging technique over solid immersion lens and confocal microscopies. *Appl. Phys. Lett.* **2014**, *104*, 061117. [CrossRef]
64. Darafsheh, A.; Guardiola, C.; Palovcak, A.; Finlay, J.C.; Cárabe, A. Optical super-resolution imaging by high-index microspheres embedded in elastomers. *Opt. Letters* **2015**, *40*, 5–8. [CrossRef] [PubMed]
65. Heifetz, A.; Kong, S.C.; Sahakian, A.V.; Taflove, A.; Backman, V. Photonic nanojets. *J. Comput. Theor. Nanosci.* **2009**, *6*, 1979–1992. [CrossRef]
66. Zhou, S.; Deng, Y.; Zhou, W.; Yu, M.; Urbach, H.P.; Wu, Y. Effects of whispering gallery mode in microsphere super-resolution imaging. *Appl. Phys. B* **2017**, *123*, 236. [CrossRef]
67. Ristori, A.; Hamilton, T.; Toliopoulos, D.; Felici, M.; Pettinari, G.; Sanguinetti, S.; Gurioli, M.; Mohseni, H.; Biccari, F. Photonic jet writing of quantum dots self-aligned to dielectric microspheres. *Adv. Quantum Technol.* **2021**, *4*, 2100045. [CrossRef]
68. Fan, X.; Zheng, W.; Singh, D.J. Light scattering and surface plasmons on small spherical particles. *Light Sci. Appl.* **2014**, *3*, e179. [CrossRef]
69. Kim, M.S.; Scharf, T.; Mühlig, S.; Rockstuhl, C.; Herzig, H.P. Engineering photonic nanojets. *Opt. Express* **2011**, *19*, 10206–10220. [CrossRef]
70. Wang, B.; Barbiero, M.; Zhang, Q.M.; Gu, M. Super-resolution optical microscope: Principle, instrumentation, and application. *Front. Inf. Technol. Electron. Eng.* **2019**, *20*, 608–630. [CrossRef]
71. Yang, H.; Trouillon, R.; Huszka, G.; Gijs, M.A. Super-resolution imaging of a dielectric microsphere is governed by the waist of its photonic nanojet. *Nano Lett.* **2016**, *16*, 4862–4870. [CrossRef]
72. Li, X.; Chen, Z.; Taflove, A.; Backman, V. Optical analysis of nanoparticles via enhanced backscattering facilitated by 3-D photonic nanojets. *Opt. Express* **2005**, *13*, 526–533. [CrossRef] [PubMed]
73. Kasim, J.; Ting, Y.; Meng, Y.Y.; Ping, L.J.; See, A.; Jong, L.L.; Xiang, S.Z. Near-field Raman imaging using optically trapped dielectric microsphere. *Opt. Express* **2008**, *16*, 7976–7984. [CrossRef] [PubMed]
74. Lecler, S.; Takakura, Y.; Meyrueis, P. Properties of a three-dimensional photonic jet. *Opt. Lett.* **2005**, *30*, 2641–2643. [CrossRef]
75. Yue, L.; Yan, B.; Monks, J.N.; Dhama, R.; Jiang, C.; Minin, O.V.; Minin, I.V.; Wang, Z. Full three-dimensional Poynting vector flow analysis of great field-intensity enhancement in specifically sized spherical-particles. *Sci. Rep.* **2019**, *9*, 20224. [CrossRef] [PubMed]
76. Lee, S.; Li, L.; Wang, Z.; Guo, W.; Yan, Y.; Wang, T. Immersed transparent microsphere magnifying sub-diffraction-limited objects. *Appl. Opt.* **2013**, *52*, 7265–7270. [CrossRef] [PubMed]
77. Du, C.; Kasim, J.; You, Y.M.; Shi, D.N.; Shen, Z.X. Enhancement of Raman scattering by individual dielectric microspheres. *J. Raman Spectrosc.* **2011**, *42*, 145–148. [CrossRef]
78. Sundaram, V.M.; Wen, S.B. Analysis of deep sub-micron resolution in microsphere based imaging. *Appl. Phys. Lett.* **2014**, *105*, 204102. [CrossRef]

79. Li, Y.; Liu, X.; Li, B. Single-cell biomagnifier for optical nanoscopes and nanotweezers. *Light Sci. Appl.* **2019**, *8*, 61. [CrossRef]
80. Minin, I.V.; Minin, O.V.; Pacheco-Peña, V.; Beruete, M. Subwavelength, standing-wave optical trap based on photonic jets. *Quantum Electron.* **2016**, *46*, 555. [CrossRef]
81. Minin, I.V.; Minin, O.V.; Cao, Y.; Liu, Z.; Geints, Y.E.; Karabchevsky, A. Optical vacuum cleaner by optomechanical manipulation of nanoparticles using nanostructured mesoscale dielectric cuboid. *Sci. Rep.* **2019**, *9*, 1–8. [CrossRef]
82. Bahng, J.H.; Jahani, S.; Montjoy, D.G.; Yao, T.; Kotov, N.; Marandi, A. Mie resonance engineering in meta-shell supraparticles for nanoscale nonlinear optics. *ACS Nano* **2020**, *14*, 17203–17212. [CrossRef]
83. Minin, I.V.; Minin, O.V.; Glinskiy, I.A.; Khabibullin, R.A.; Malureanu, R.; Lavrinenko, A.V.; Yakubovsky, D.I.; Arsenin, A.V.; Volkov, V.S.; Ponomarev, D.S. Plasmonic nanojet: An experimental demonstration. *Opt. Lett.* **2020**, *45*, 3244–3247. [CrossRef] [PubMed]
84. Xu, K.; Jiang, C.; Chen, P.; Wang, W.; Zhang, Z. Miniature self-mixing interferometer based on a microsphere superlens for microactuator displacement measurement. *Opt. Commun.* **2021**, *498*, 127212. [CrossRef]
85. Zhou, Y.; Hong, M. Formation of a three-dimensional bottle beam via an engineered microsphere. *Photonics Res.* **2021**, *9*, 1598–1606. [CrossRef]
86. Minin, I.V.; Geints, Y.E.; Zemlyanov, A.A.; Minin, O.V. Specular-reflection photonic nanojet: Physical basis and optical trapping application. *Opt. Express* **2020**, *28*, 22690–22704. [CrossRef]
87. Yue, L.; Yan, B.; Monks, J.N.; Dhama, R.; Wang, Z.; Minin, O.V.; Minin, I.V. A millimetre-wave cuboid solid immersion lens with intensity-enhanced amplitude mask apodization. *J. Infrared Milli. Terahz. Waves* **2018**, *39*, 546–552. [CrossRef]
88. Nguyen Pham, H.H.; Hisatake, S.; Minin, O.V.; Nagatsuma, T.; Minin, I.V. Enhancement of spatial resolution of terahertz imaging systems based on terajet generation by dielectric cube. *Appl. Photonics* **2017**, *2*, 056106. [CrossRef]
89. Minin, I.V.; Minin, O.V. Terahertz artificial dielectric cuboid lens on substrate for super-resolution images. *Opt. Quantum Electron.* **2017**, *49*, 326. [CrossRef]
90. Ang, A.S.; Karabchevsky, A.; Minin, I.V.; Minin, O.V.; Sukhov, S.V.; Shalin, A.S. 'Photonic Hook' based optomechanical nanoparticle manipulator. *Sci. Rep.* **2018**, *8*, 2029. [CrossRef] [PubMed]
91. Zhu, J.; Goddard, L.L. Spatial control of photonic nanojets. *Opt. Express* **2016**, *24*, 30444–30464. [CrossRef]
92. Gu, G.; Zhou, R.; Chen, Z.; Xu, H.; Cai, G.; Cai, Z.; Hong, M. Super-long photonic nanojet generated from liquid-filled hollow microcylinder. *Opt. Lett.* **2015**, *40*, 625–628. [CrossRef]
93. Minin, I.V.; Minin, O.V.; Geints, Y.E.; Panina, E.K.; Karabchevsky, A. Optical manipulation of micro-and nanoobjects based on structured mesoscale particles: A brief review. *Atmos. Oceanic Opt.* **2020**, *33*, 464–469. [CrossRef]
94. Cao, Y.; Liu, Z.; Minin, O.V.; Minin, I.V. Deep subwavelength-scale light focusing and confinement in nanohole-structured mesoscale dielectric spheres. *Nanomaterials* **2019**, *9*, 186. [CrossRef]
95. Minin, I.V.; Minin, O.V. Recent trends in optical manipulation inspired by mesoscale photonics and diffraction optics. *J. Biomed. Photonics Eng.* **2020**, *6*, 020301. [CrossRef]
96. Minin, O.V.; Minin, I.V.; Cao, Y. Optical magnet for nanoparticles manipulations based on optical vacuum cleaner concept. Saratov Fall Meeting 2020: Optical and Nanotechnologies for Biology and Medicine. *Int. Soc. Opt. Photonics* **2021**, *11845*, 118451G. [CrossRef]
97. Bekirov, A.R.; Luk'yanchuk, B.S.; Fedyanin, A.A. Virtual image within a transparent dielectric sphere. *JETP Lett.* **2020**, *112*, 341–345. [CrossRef]
98. Wang, Z.; Luk'yanchuk, B.; Yue, L.; Yan, B.; Monks, J.; Dhama, R.; Minin, O.V.; Minin, I.V.; Huang, S.; Fedyanin, A.A. High order Fano resonances and giant magnetic fields in dielectric microspheres. *Sci. Rep.* **2019**, *9*, 20293. [CrossRef] [PubMed]
99. Huckabay, H.A.; Wildgen, S.M.; Dunn, R.C. Label-free detection of ovarian cancer biomarkers using whispering gallery mode imaging. *Biosens. Bioelectron.* **2013**, *45*, 223–229. [CrossRef]
100. Gerard, D.; Wenger, J.; Devilez, A.; Gachet, D.; Stout, B.; Bonod, N.; Popov, E.; Rigneault, H. Strong electromagnetic confinement near dielectric microspheres to enhance single-molecule fluorescence. *Opt. Express* **2008**, *16*, 15297–15303. [CrossRef]
101. Aouani, H.; Schon, P.; Brasselet, S.; Rigneault, H.; Wenger, J. Two-photon fluorescence correlation spectroscopy with high count rates and low background using dielectric microspheres. *Biomed. Opt. Express* **2010**, *1*, 1075–1083. [CrossRef] [PubMed]
102. Yang, H.; Cornaglia, M.; Gijs, M.A. Photonic nanojet array for fast detection of single nanoparticles in a flow. *Nano Lett.* **2015**, *15*, 1730–1735. [CrossRef]
103. Lu, D.; Pedroni, M.; Labrador-Páez, L.; Marqués, M.I.; Jaque, D.; Haro-González, P. Nanojet trapping of a single sub-10 nm upconverting nanoparticle in the full liquid water temperature range. *Small* **2021**, *17*, 2006764. [CrossRef] [PubMed]
104. Xin, H.; Xu, R.; Li, B. Optical trapping, driving and arrangement of particles using a tapered fibre probe. *Sci. Rep.* **2012**, *2*, 818. [CrossRef] [PubMed]
105. Xin, H.; Li, Y.; Liu, X.; Li, B. Escherichia coli-based biophotonic waveguides. *Nano Lett.* **2013**, *13*, 3408–3413. [CrossRef] [PubMed]
106. Lin, L.; Kollipara, P.S.; Kotnala, A.; Jiang, T.; Liu, Y.; Peng, X.; Korgel, B.A.; Zheng, Y. Opto-thermoelectric pulling of light-absorbing particles. *Light Sci. Appl.* **2020**, *9*, 34. [CrossRef]
107. Xin, H.; Li, Y.; Xu, D.; Zhang, Y.; Chen, C.H.; Li, B. Single upconversion nanoparticle–bacterium cotrapping for single–bacterium labeling and analysis. *Small* **2017**, *13*, 1603418. [CrossRef] [PubMed]

108. Xin, H.; Li, B. Optical orientation and shifting of a single multiwalled carbon nanotube. *Light Sci. Appl.* **2014**, *3*, e205. [CrossRef]
109. Li, Y.C.; Xin, H.B.; Lei, H.X.; Liu, L.L.; Li, Y.Z.; Zhang, Y.; Li, B.J. Manipulation and detection of single nanoparticles and biomolecules by a photonic nanojet. *Light Sci. Appl.* **2016**, *5*, e16176. [CrossRef] [PubMed]
110. Gérard, D.; Devilez, A.; Aouani, H.; Stout, B.; Bonod, N.; Wenger, J.; Popov, E.; Rigneault, H. Efficient excitation and collection of single-molecule fluorescence close to a dielectric microsphere. *J. Opt. Soc. Am. B* **2009**, *26*, 1473–1478. [CrossRef]
111. Li, Y.; Xin, H.; Zhang, Y.; Lei, H.; Zhang, T.; Ye, H.; Saenz, J.J.; Qiu, C.W.; Li, B. Living nanospear for near-field optical probing. *ACS Nano* **2018**, *12*, 10703–10711. [CrossRef] [PubMed]
112. Xin, H.; Li, Y.; Li, B. Controllable patterning of different cells via optical assembly of 1D periodic cell structures. *Adv. Funct. Mater.* **2015**, *25*, 2816–2823. [CrossRef]
113. Li, Y.; Liu, X.; Xu, X.; Xin, H.; Zhang, Y.; Li, B. Red-blood-cell waveguide as a living biosensor and micromotor. *Adv. Funct. Mater.* **2019**, *29*, 1905568. [CrossRef]
114. Li, Y.; Liu, X.; Yang, X.; Lei, H.; Zhang, Y.; Li, B. Enhancing upconversion fluorescence with a natural bio-microlens. *ACS Nano* **2017**, *11*, 10672–10680. [CrossRef]
115. Chen, X.; Wu, T.; Gong, Z.; Li, Y.; Zhang, Y.; Li, B. Subwavelength imaging and detection using adjustable and movable droplet microlenses. *Photonics Res.* **2020**, *8*, 225–234. [CrossRef]
116. Devilez, A.; Bonod, N.; Stout, B. Near field dielectric microlenses. *Proc. SPIE* **2010**, *7717*, 771708. [CrossRef]
117. Yang, S.; Taflove, A.; Backman, V. Experimental confirmation at visible light wavelengths of the backscattering enhancement phenomenon of the photonic nanojet. *Opt. Express* **2011**, *19*, 7084–7093. [CrossRef]
118. Li, Y.; Xin, H.; Liu, X.; Zhang, Y.; Lei, H.; Li, B. Trapping and detection of nanoparticles and cells using a parallel photonic nanojet array. *ACS Nano* **2016**, *10*, 5800–5808. [CrossRef]
119. Yi, K.J.; Wang, H.; Lu, Y.F.; Yang, Z.Y. Enhanced Raman scattering by self-assembled silica spherical microparticles. *J. Appl. Phys.* **2007**, *101*, 063528. [CrossRef]
120. Dantham, V.R.; Bisht, P.B.; Namboodiri, C.K.R. Enhancement of Raman scattering by two orders of magnitude using photonic nanojet of a microsphere. *J. Appl. Phys.* **2011**, *109*, 103103. [CrossRef]
121. Xing, C.; Yan, Y.; Feng, C.; Xu, J.; Dong, P.; Guan, W.; Zeng, Y.; Zhao, Y.; Jiang, Y. Flexible Microsphere-embedded film for microsphere-enhanced Raman spectroscopy. *ACS Appl. Mater. Interfaces* **2017**, *9*, 32896–32906. [CrossRef]
122. Arya, A.; Laha, R.; Das, G.M.; Dantham, V.R. Enhancement of Raman scattering signal using photonic nanojet of portable and reusable single microstructures. *J. Raman Spectrosc.* **2018**, *49*, 897–902. [CrossRef]
123. Gašparić, V.; Ristić, D.; Gebavi, H.; Ivanda, M. Resolution and signal enhancement of Raman mapping by photonic nanojet of a microsphere. *Appl. Surf. Sci.* **2021**, *545*, 149036. [CrossRef]
124. Kang, D.; Pang, C.; Kim, S.M.; Cho, H.S.; Um, H.S.; Choi, Y.W.; Suh, K.Y. Shape-controllable microlens arrays via direct transfer of photocurable polymer droplets. *Adv. Mater.* **2012**, *24*, 1709–1715. [CrossRef]
125. Lee, J.Y.; Hong, B.; Kim, W.Y.; Min, S.K.; Kim, Y.; Jouravlev, M.V.; Bose, R.; Kim, K.S.; Hwang, I.C.; Kaufman, L.J.; et al. Near-field focusing and magnification through self-assembled nanoscale spherical lenses. *Nature* **2009**, *460*, 498–501. [CrossRef]
126. Murade, C.U.; Ende, V.D.; Mugele, F.G. High speed adaptive liquid microlens array. *Opt. Express* **2012**, *20*, 18180–18187. [CrossRef] [PubMed]
127. Bogucki, A.; Zinkiewicz, Ł.; Grzeszczyk, M.; Pacuski, W.; Nogajewski, K.; Kazimierczuk, T.; Rodek, A.; Suffczyński, J.; Watanabe, K.; Taniguchi, K.; et al. Ultra-long-working-distance spectroscopy of single nanostructures with aspherical solid immersion microlenses. *Light Sci. Appl.* **2020**, *9*, 48. [CrossRef] [PubMed]
128. Lee, S.; Li, L. Rapid super-resolution imaging of sub-surface nanostructures beyond diffraction limit by high refractive index microsphere optical nanoscopy. *Opt. Commun.* **2015**, *334*, 253–257. [CrossRef]
129. Fan, W.; Yan, B.; Wang, Z.; Wu, L. Three-dimensional all-dielectric metamaterial solid immersion lens for subwavelength imaging at visible frequencies. *Sci. Adv.* **2016**, *2*, e1600901. [CrossRef] [PubMed]
130. Dhama, R.; Yan, B.; Palego, C.; Wang, Z. Super-Resolution imaging by dielectric superlenses: TiO_2 metamaterial superlens versus $BaTiO_3$ superlens. *Photonics* **2021**, *8*, 222. [CrossRef]
131. Monks, J.N.; Yan, B.; Hawkins, N.; Vollrath, F.; Wang, Z. Spider silk: Mother nature's bio-superlens. *Nano Lett.* **2016**, *16*, 5842–5845. [CrossRef]
132. Li, J.; Liu, W.; Li, T.; Rozen, I.; Zhao, J.; Bahari, B.; Kante, B.; Wang, J. Swimming microrobot optical nanoscopy. *Nano Lett.* **2016**, *16*, 6604–6609. [CrossRef]
133. Zhou, J.; Lian, Z.; Zhou, C.; Bi, S.; Wang, Y. Scanning microsphere array optical microscope for efficient and large area super-resolution imaging. *J. Opt.* **2020**, *22*, 105602. [CrossRef]
134. Wen, Y.; Yu, H.; Zhao, W.; Li, P.; Wang, F.; Ge, Z.; Wang, X.; Liu, L.; Li, W.J. Scanning super-resolution imaging in enclosed environment by laser tweezer controlled superlens. *Biophys. J.* **2020**, *119*, 2451–2460. [CrossRef]
135. Krivitsky, L.A.; Wang, J.J.; Wang, Z.; Luk'yanchuk, B. Locomotion of microspheres for super-resolution imaging. *Sci. Rep.* **2013**, *3*, 3501. [CrossRef] [PubMed]
136. Wang, S.; Zhang, D.; Zhang, H.; Han, X.; Xu, R. Super-resolution optical microscopy based on scannable cantilever-combined microsphere. *Microsc. Res. Tech.* **2015**, *78*, 1128–1132. [CrossRef]

137. Allen, K.W.; Farahi, N.; Li, Y.; Limberopoulos, N.I.; Walker, D.E., Jr.; Urbas, A.M.; Liberman, V.; Astratov, V.N. Super-resolution microscopy by movable thin-films with embedded microspheres: Resolution analysis. *Ann. Phys.* **2015**, *527*, 513–522. [CrossRef]
138. Zhang, T.; Li, P.; Yu, H.; Wang, F.; Wang, X.; Yang, T.; Yang, W.; Li, W.J.; Wang, Y.; Liu, L. Fabrication of flexible microlens arrays for parallel super-resolution imaging. *Appl. Surf. Sci.* **2020**, *504*, 144375. [CrossRef]
139. Yan, Y.; Li, L.; Feng, C.; Guo, W.; Lee, S.; Hong, M. Microsphere-coupled scanning laser confocal nanoscope for sub-diffraction-limited imaging at 25 nm lateral resolution in the visible spectrum. *ACS Nano* **2014**, *8*, 1809–1816. [CrossRef] [PubMed]
140. Yang, H.; Moullan, N.; Auwerx, J.; Gijs, M.A. Super-resolution biological microscopy using virtual imaging by a microsphere nanoscope. *Small* **2014**, *10*, 1712–1718. [CrossRef]
141. Chernomyrdin, N.V.; Kucheryavenko, A.S.; Kolontaeva, G.S.; Katyba, G.M.; Karalkin, P.A.; Parfenov, V.A.; Gryadunova, A.A.; Norkin, N.E.; Smolyanskaya, O.A.; Minin, O.V.; et al. A potential of terahertz solid immersion microscopy for visualizing sub-wavelength-scale tissue spheroids. *Proc. SPIE* **2018**, *10677*, 106771Y. [CrossRef]
142. Wang, F.; Liu, L.; Yu, H.; Wen, Y.; Yu, P.; Liu, Z.; Wang, Y.; Li, W.J. Scanning superlens microscopy for non-invasive large field-of-view visible light nanoscale imaging. *Nat. Commun.* **2016**, *7*, 13748. [CrossRef] [PubMed]